On the dielectric behavior of annealed plasma sprayed forsterite and alumina coatings

Lamarre, Jean-Michel; Cojocaru, Cristian V.; Legoux, Jean-Gabriel; National Research Council of Canada

Publisher's version / Version de l'éditeur:

Proceedings of the International Thermal Spray Conference 2014 (ITSC), pp. 184-189, 2014-05-21

On the dielectric behavior of annealed plasma sprayed forsterite and alumina coatings

Jean-Michel Lamarre, Cristian V. Cojocaru and Jean-Gabriel Legoux, National Research Council of Canada, Boucherville, QC, Canada

Atmospheric plasma spray (APS) is an efficient technique for depositing high performance dielectric coatings at a low cost, with high deposition rate and on complex-shaped parts. Due to its availability, low price, ease to spray and good dielectric properties, alumina (Al_2O_3) is a very common choice of material for insulating applications. However, the coefficient of thermal expansion (CTE) of alumina does not represent the best match for the CTE of most metallic substrates hence alternative high CTE ceramic materials are of interest. We report on the microstructural and electrical properties of a dense high CTE forsterite (Mg_2SiO_4) coating deposited by APS. Annealed forsterite coatings' microstructure and dielectric properties are compared to that of annealed alumina coatings. The ceramics' electrical properties were evaluated by performing impedance measurements on as-sprayed coatings and coatings exposed to different annealing temperatures. We show that both materials exhibit important degradation after exposure to a threshold temperature. An equivalent electrical model is used to extract relevant coating properties such as resistivity and dielectric constant. The coating electrical degradation mechanisms are discussed.

1 Introduction

Dielectric and electrically insulating coatings are used in a wide variety of industrial applications as for example in the automotive, aerospace, oil and gas, medical, electrical and electronics industries. Among other fabrication techniques, atmospheric plasma spray (APS) offers the advantages of being versatile, efficient, inexpensive and allows coating of large and complex surfaces [1]. Due to its availability, cheap price, ease to spray and good dielectric properties, alumina (Al_2O_3) is a very common choice of material for insulating applications. APS alumina electrical properties and mechanical performance have been studied by many authors over the last decades. Alumina optimized spray parameters can thus readily be obtained from the literature. In the context of electrical applications, particular attention has been given to the study of the relationship between the coating's microstructure and the resulting electrical performance in terms of resistivity, dielectric constant, loss tangent and dielectric strength [2].

While alumina is suitable for most applications, the need exists for a high performance dielectric coating (e.g. high dielectric strength and resistivity) possessing a CTE matching that of metallic substrates for medium and high temperature applications. Indeed, in this case, alumina coefficient of expansion is too low and thus unsuitable. In a previous paper [3], we identified forsterite as a potential dielectric material satisfying the aforementioned required properties. We demonstrated the feasibility of spraying good quality forsterite coatings by using an appropriate powder and optimized spray parameters. Room temperature results for as-sprayed coating resistivity, dielectric constant and dielectric strength were reported.

High temperature applications require the dielectric material to retain sufficient electrical insulation at high temperatures. In addition, the coating should not suffer from degradation over time and cycling. Motivated by these aspects, first experimental electric measurement trials on annealed alumina and forsterite coatings deposited on mild steel substrates were undertaken. The measurements were accomplished using electric impedance spectroscopy as this technique was used successfully by many authors to determine the electrical properties of thermally sprayed coatings and other relevant materials [4-15]. Measurements performed at room temperature revealed a strong decrease in performance of the alumina and forsterite coatings after annealing which was ascribed to water absorption. This was supported by much better coating performance at 125°C. It was established by other authors that γ phase alumina is strongly hygroscopic. Water absorption in thermally sprayed alumina due to air humidity is known to be detrimental to its resistivity [2, 7, 16]. However, a low amount of data is available on the electrical performance of annealed forsterite and forsterite coatings [17]. This paper will thus focus on the characterization, the modelling and the comparison of the room temperature electrical properties of annealed forsterite and alumina coatings.

2 Experimental Methodology

2.1 Coating Deposition

Mild steel 3x3 inches substrates were first degreased using acetone and grit blasted with 60 mesh alumina grit. 275-325 µm thick alumina and forsterite coatings were plasma sprayed using a Sulzer-Metco F4 torch. Three samples were sprayed for each material using one optimized condition per material (alumina A1, A2, A3 and forsterite F1, F2, F3).The spray parameters were selected such as to minimize coating porosity while maintaining good coating adhesion and high deposition efficiency. Table 1 presents a comprehensive list of the used spray parameters. Following the dielectric deposition, a square FeCrAl electrode (area of 1.4×10^{-2} m^2) was thermally sprayed onto the dielectric layer. This top coating is used as an electrode for the electrical measurements. It allows a good and repetitive contact without possible issues pertaining to external electrodes such as air gaps.

Table 1. Summary of the alumina and forsterite plasma spray deposition parameters.

Parameter	Alumina	Forsterite
Current	600 A	600 A
Voltage	65 V	54V
Primary gas flow	41 l/min Ar	40 l/min Ar
Secondary gas flow	14 l/min H_2	10 l/min H_2
Carrier gas flow	6 l/min Ar	4.5 l/min Ar
Powder feed rate	24 g/min	18 g/min
Stand-off	12.5 cm	10.0 cm

2.2 Annealing and Measurement Sequence

As-sprayed samples were first electrically characterized (see section 2.3) after post-deposition cool down in a room with controlled temperature (25°C) and humidity levels (40%). Samples were then submitted to a serie of 1-hour annealing treatments at the following temperatures: 149°C (300°F), 204°C (400°F), 260°C (500°F), 316°C (600°F), 343°C (650°F), 371°C (700°F), 399°C (750°F) and 427°C (800°F). After each heat treatment, the samples were placed in the aforementioned controlled condition room for cool down and humidity conditioning and were then electrically measured. The electrical characterization was performed under controlled environment to avoid possible shifts in data due to variations of temperature or humidity.

2.3 Electrical measurements

The electrical measurements were carried out using a potentiostat (Princeton Applied Research EG&G, Model 263A, Oak Ridge, TN, USA) and a frequency response detector (Model 1025). Data acquisition was performed using the PowerSuite software from the same company. The measurement range was set between 30 and 100 kHz with an AC probing voltage of 100 mV.

An electrical element model was fitted to Nyquist data (*Im Z* vs *Re Z*) using a standard least-mean-square algorithm with a weighting function. The weighting function is rendered necessary by the difference of several orders of magnitude between the low and high frequency impedances. Incorrect weighting of the points would results in a fit neglecting the high frequency behaviour of the system. The following error function was used for the *n* data points:

$$E = \sum_{i=1}^{n} \frac{\left[Re(Z_M^i) - Re(Z_E^i)\right]^2 + \left[Im(Z_M^i) - Im(Z_E^i)\right]^2}{\left[\left|Re(Z_E^i)\right| + \left|Im(Z_E^i)\right|\right]^{1/2}}$$

where the indices *M* and *E* stands for the model and experimental impedance respectively.

2.4 Electrical model

Early microstructural characterization indicated that a simple parallel *RC* circuit was not appropriate to describe the observed microstructures. Indeed, the presence of cracks and defects in the coatings cannot be taken into account by this model. Trials confirmed that a fit using a simple parallel *RC* circuit was impossible. A two time constants electrical model was used as schematized in figure 1. The use of two *RC* elements in the circuit leads to the presence of two semi-circles in the Nyquist plots. From a material point of view, the different circuit elements are associated with the following quantities: the coating capacitance C_c, the pore resistance R_{po}, the double layer capacitance C_{dl} and the interfacial polarization resistance R_t. The coating capacitance is a simple function of the coating geometry (area *A* and thickness *d*) and relative dielectric constant (ε):

$$\varepsilon = \frac{C_c d}{\varepsilon_0 A}.$$

R_{po} is the coating resistance associated with the electrical conduction of absorbed water on the pores' surface. It is worth mentioning that this resistance is typically much smaller than the bulk resistance of the dielectric materials. The bulk resistance can thus be omitted in the electrical model. The effective coating resistivity (ρ_{eff}) can be extracted from the following equation:

$$\rho_{eff} = \frac{R_{po} A}{d}.$$

Finally, the double layer capacitance and the interfacial polarization resistance arise from the absorption of water and the reactions at the metallic substrate surface [8, 14, 15]. The effects of humidity and water on the model parameters are the following:

1) The coating capacity increases as water is absorbed in the coating.
2) The interfacial polarization resistance decreases and double layer capacitance increases as a higher percentage of the substrate is exposed to water.
3) The pore resistance decreases as water is absorbed on the exposed porosity surface.

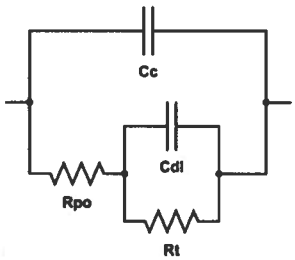

Fig. 1. Diagram of the equivalent electrical circuit used in the electrical model. C_c, C_{dl}, R_{po}, and R_t stand respectively for, the coating capacitance, the double layer capacitance, the pore resistance, and the interfacial polarization resistance.

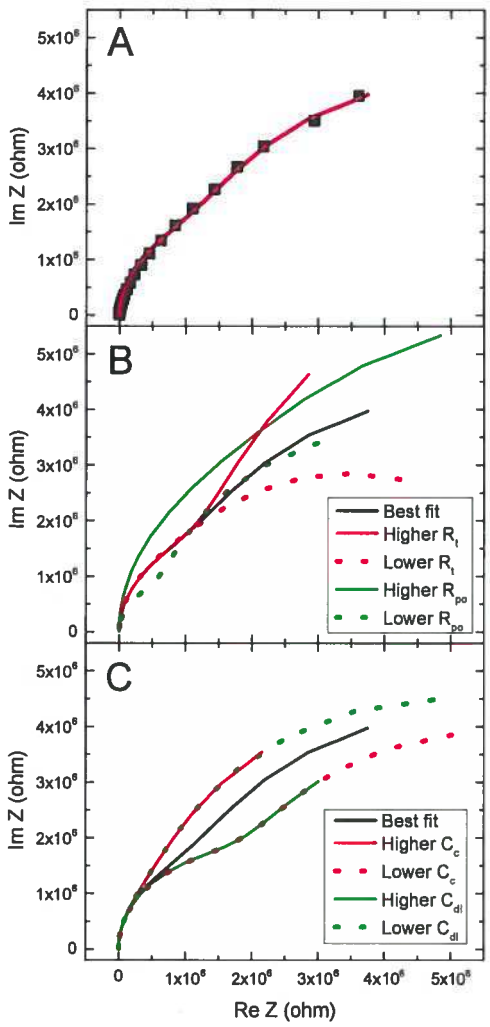

Fig. 2. A) Example of a Nyquist plot for alumina sample A2. The experimental data are indicated by black dots while the best model fit is indicated by the red line. B) and C): Effect of varying the various parameters of the model. The designation *Higher* corresponds to doubling the parameter compared to the best fit value while the designation *Lower* corresponds to a reduction of 50% of the parameter.

Note that the impedance of the top electrode and the substrate are neglected in our model as their values are very small (few ohms) compared to that of the other circuit elements.

An example of a typical Nyquist fit is presented in figure 2A for alumina sample A2. Notice that the fit is adequate both in the low and high frequency range. One typical area of concern in electrical impedance spectroscopy is the model validity and the uniqueness of the solution. In order to address that last point, figure 2B and 2C were plotted to show the effect of modifying individually the model parameters. Comparing the effect of varying R_{po} and R_t, one can readily observe that the effect of varying R_t is important at low frequencies but negligible at higher frequencies. Indeed, *Im Z* increases significantly with R_t at low frequencies. This is of course a consequence of the optimal capacitance values and the respective diameter of the two *RC* Nyquist semi-circles. Switching to the effect of the pore resistance, one can notice that increasing R_{po} increases *Im Z* over the whole frequency range differentiating its effect for that of R_t. An increase in one or both resistances increases the total impedance and increases the corresponding semi-circles radiuses. One can also notice that an increase in R_{po} increases the length of the impedance curve while reducing it reduces the same length. Varying R_t does the opposite. The effects of varying the capacitances C_c and C_{dl} are very different even if they look similar at first glance. Increasing C_c increases the imaginary part of the impedance while increasing C_{dl} decreases it. Notice also the dissimilar lengths of the impedance curves of the otherwise similar higher C_c vs lower C_{dl} and lower C_c vs higher C_{dl}. One can conclude that all four parameters have a distinct effect on the impedance curve. Trials and errors have shown that the fitting procedure easily converge to a solution provided that a decent choice of initial parameters is made.

3 Results and Discussion

3.1 Coating Microstructure

Alumina and forsterite microstructures for as-sprayed and after annealing coatings are presented in figure 3. Both as-sprayed dielectrics exhibit dense structures. Low magnification pictures of both materials are shown in figure 3A and 3B. Alumina and forsterite exhibit similar porosity levels with forsterite being slightly more porous. However, upon inspection at higher magnification, alumina and forsterite coating's microstructure proved to be very different. The main difference between the two materials is the presence or absence of visible splat boundaries. As can be observed from figure 3D, the forsterite sample shows the presence of large particles embedded in a well-bounded matrix where splat boundaries are not very well defined. Forsterite coatings also possess long vertical cracks (indicated by white arrows) which are likely detrimental to the electrical insulating properties. On the other end, alumina microstructure as shown in figure 3C, while being somehow more uniform, exhibit very well-defined splat boundaries. These boundaries can represent possible channels for humidity to penetrate in the coating. This situation is illustrated schematically in figure 4. In this scenario, water condensates into the hygroscopic surfaces located in the intersplat boundaries or vertical cracks. The dielectric electrical performance is drastically reduced if the pore network architecture allows for connected cracks/boundaries connecting the coating surface and the substrate.

Figure 3 E) and F) present respectively the microstructure of annealed alumina and annealed forsterite. The microstructures were obtained after the

sample A2 (alumina) and F2 (forsterite) had completed the annealing sequence (see section 2.2). No major differences are observed between the as-sprayed and annealed coatings for both materials. It is worthwhile to notice that forsterite coating long vertical cracks can still be observed.

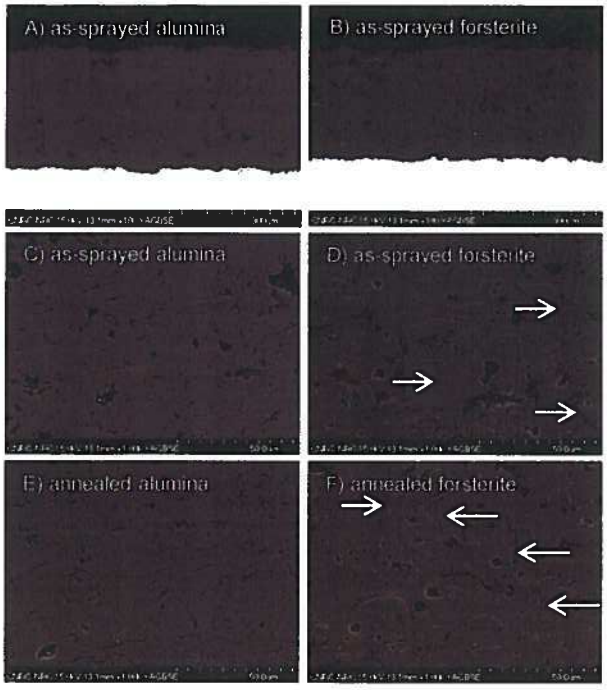

Fig. 3. Microstructural SEM pictures of the A) and C) as sprayed alumina coating, B) and D) as sprayed forsterite coating, E) annealed alumina coating, and F) annealed forsterite coating. White arrows indicate some vertical cracks.

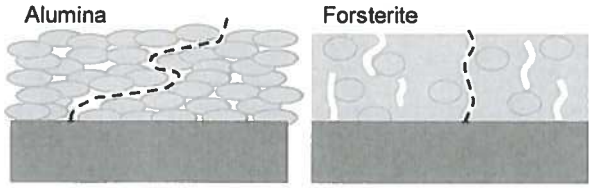

Fig.4. Schematic representation of the dielectric coating microstructures. Alumina: the dashed line indicates connected open intersplat boundaries linking the upper electrode and the substrate. Forsterite: the dashed line indicates a vertical crack connecting the upper electrode and the substrate.

3.2 Electrical Properties

Figure 5 presents the evolution of the best fit model parameters as a function of the temperature for alumina A1 and forsterite F1 samples. Other alumina (A2 and A3) and forsterite (F2 and F3) behave very similarly. For temperatures below 300°C, the alumina pore resistance (R_{po}) and interfacial polarization resistance (R_t) increase while the double–layer capacitance (C_{dl}) decreases. Because of the alumina high hygroscopicity, it is likely that the water content in the coating is high in the initial stage. The observed parameter trends are consistent with a decrease of the coating water content during the first annealing step. Indeed, the presence of water on the pore surface provides conduction channels along the coating thickness reducing R_{po}. As described in section 2.4, the exposure of the substrate to air humidity increase C_{dl} and decrease R_t which are respectively proportional and inversely proportional to the exposed area. This is also in accordance with the alumina microstructure showing a large number of well-defined openings in the splat boundaries. Furthers improvements of the alumina properties after the first annealing step points out towards structural changes that will be discussed later on. Forsterite coating, on the other hand, did not exhibit this low temperature annealing effect possibly indicating a lower initial absorption of water and less structural changes consistent with the low amount of open splat boundaries observed in the microstructure.

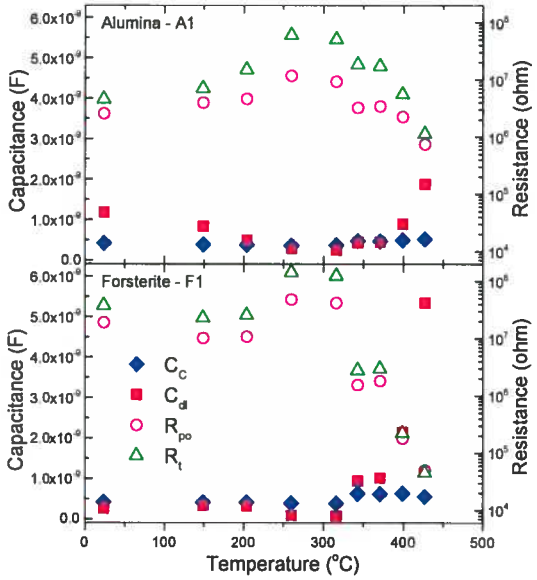

Fig. 5. Evolution as of function of the temperature of the fitted parameters (C_c, C_{dl}, R_t and R_{po}) for alumina coating A1 (top) and forsterite coating F1 (bottom).

The aforementioned model observations are reflected in the calculated coating resistivities (figure 6) and calculated coating relative dielectric constants (figure 7). Indeed, as-sprayed forsterite resistivity is an order of magnitude higher than that of as-sprayed alumina. The more compact intersplat structure of the forsterite coating most likely explains this result. Alumina relative dielectric constant decreases with temperature while forsterite relative dielectric is constant. The decrease of the alumina dielectric constant from as-sprayed to the first annealing temperatures can most likely be attributed to a lower water content (water relative dielectric constant = 78).

At temperature above 300°C, both alumina and forsterite exhibits a sharp increase in double layer capacitance and a dramatic decrease in both R_{po} and R_t. Meanwhile, the coating capacitance increases. Both materials exhibit a sharp resistivity decrease while their relative dielectric constant follows the inverse trend. The forsterite resistivity decreases by almost three orders of magnitude between annealing temperatures of 316°C to 427°C. It is worth noticing that forsterite sample F3 outperforms samples F1 and F2 between 300°C and 400°C. Its performance is similar to that of the two other samples at 427°C. The alumina seemingly resists better to high temperature annealing as its resistivity is only decreasing by one order of magnitude in the same temperature range. Both materials relative constant increase significantly which is a clear indication that water is absorbed. Based on these observations, it is clear that the coatings are suffering from structural damage when annealing temperature reaches 300°C.

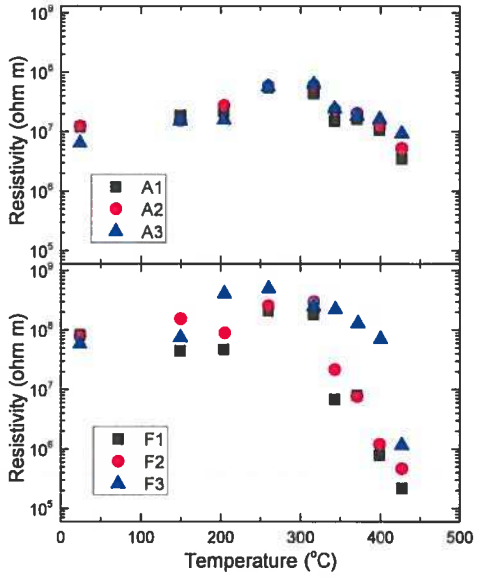

Fig. 6. Evolution as a function of the temperature of the resistivity of the alumina (top) and forsterite coatings (bottom).

3.3 Mechanisms

Alumina and forsterite coatings CTEs differ from that of the mild steel substrate (and top electrode). During annealing, this CTE difference causes the intersplat boundaries to move. Upon cooling, the intersplat areas reorganize as the coating and substrate contract to their initial length. Annealing is known to reduce the deposition stresses. It is thus likely that the final structure after cooling is slightly more compact thus decreasing the intersplat distances. The critical parameter driving coating electrical performance is the extend of the connected porosity network. Minor changes in the total number of channels connecting the coating surface to the substrate has a major influence as the bulk resistivity is much higher than the pore resistivity. In the case of alumina, the relative dielectric constant is reduced since water cannot enter as deeply in the intersplat pore network.

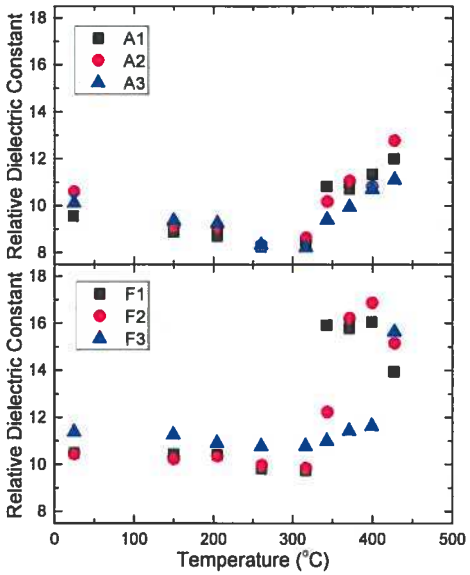

Fig. 7. Evolution as a function of the temperature of the relative dielectric constant of alumina (top) and forsterite coating (bottom).

When the annealing temperature is increased, the deformation of the dielectric coating gets more important. At a certain critical temperature which depends on the thermo-mechanical characteristics of the dielectric and the substrate, the coating will start to show permanent damage. This damage can be of three different natures: 1) intersplat boundaries do not completely close because of a too large displacement and/or 2) formation of microcracks in the dielectric layer, 3) increase of the connected open porosity network density. Unfortunately, no damage could readily be observed from the coating SEM pictures (figure 3). Nevertheless, observing such damage could be subtle as it is difficult to quantify the connected open porosity network density from 2D pictures. Forsterite high temperature inferior behavior is likely due to the high density of long vertical cracks (50 µm) increasing dramatically the likelihood of formation of relatively direct critical surface to substrate paths in the case of coating damage. The random distribution and appearance of cracks could potentially explain the better performance of sample F3 in the temperature range between 300°C and 400°C. Alumina performance should decrease more gradually since the length of the vertical defects is limited to the dimension of the splats (5 µm) limiting the appearance of straight surface to substrate paths.

3 Conclusion

Low porosity alumina and forsterite coatings were produced using the plasma spray deposition technique. A four-parameter electrical model was successfully used to model the room-temperature

electrical properties of annealed alumina and forsterite coatings. It has been shown that the absorption of water inside the intersplat boundaries and vertical cracks is likely responsible for the decrease of performance of the dielectric coatings. For as sprayed coatings and coatings annealed at low temperatures (below 300°C), the electrical resistivity of forsterite is about an order of magnitude higher than that of alumina. This was attributed to lower water absorption. This is consistent with the fact that the dielectric constant of the alumina coatings decreases with annealing while that of forsterite is stable for annealing temperatures below 300°C. After annealing at high temperature (above 300°C), both kind of coating suffers from an important decrease in performance. The resistivity of the forsterite coatings drops by 3 orders of magnitude while that of alumina decreases by 1 order of magnitude after annealing at 430°C. The inferior performance of forsterite coating can be caused by the presence of vertical cracks in the as-sprayed coatings. In light of the obtained results, forsterite is a suitable dielectric replacement for alumina for low temperature applications. Further thermal experimentation is needed to determine whether forsterite coatings could be optimized to improve their high temperatures behaviour.

4 Acknowledgements

The authors would like to acknowledge the work of Jean-Claude Tremblay (plasma spraying), David de Lagrave (characterization), Bernard Harvey (characterization) and Michel Thibodeau (SEM) and Karine Théberge (SEM).

5 Bibliography

[1] Davis, J.R. and others, Handbook of Thermal Spray Technology, ASM International, Materials Park, OH, (2004).

[2] Pawlowski, L., The Relationship Between Structure and Dielectric Properties in Plasma-Sprayed Alumina Coatings, Surf. Coat. Technol., 35 (1988), pp. 285/298.

[3] Cojocaru, C.V. , Lamarre, J.-M., Legoux, J.-G., and Marple, B.R., Atmospheric Plasma Sprayed Forsterite (Mg_2SiO_4) Coatings: An Investigation of the Processing-Microstructure-Performance Relationship, J. Therm. Spray Technol. 22, (2012), Issue 2-3, pp. 145/151.

[4] Wu, N.Q., Ogawa, K., Chyu, M., and Mao, S.X., Failure Detection of Thermal Barrier Coatings Using Impedance Spectroscopy, Thin Solid Films 457, (2004), pp. 301/306.

[5] Song, S., and Xiao, P., An Impedance Spectroscopy Study of High-temperature Oxidation of Thermal Barrier Coatings, Mat. Sci. Eng. B97, (2003), pp. 46/53.

[6] Ogawa, K., Minkov, D., Shoji, T., Sato, M., and Hashimoto, H., NDE of Degration of Thermal Barrier Coating by Means of Impedance Spectroscopy, NDT&E International 32, (1999), pp. 177/185.

[7] Favre, F., Villieras, F., Duval, Y., McRae, E., and Rapin, C., Influence of Relative Humidity on Electrical Properties of α-Al_2O_3 Powders: Resistivity and Electrochemical Impedance Spectroscopy, J. of Coll. Int. Sci. 286, (2005), pp. 615/620.

[8] Antou, G., Montavon G., Hlawka, F., Comet, A., and Coddet, C., Exploring Thermal Spray Gray Alumina Coating Pore Network Architecture by Combining Stereological Protocols and Impedance Electrochemical Spectroscopy, J. Therm. Spray Technol. 15, (2006), Issue 4, pp. 765/772.

[9] Zhu Y., and Ding, C., Characterization of Plasma Sprayed Nano-titania coatings by Impedance Spectroscopy, J. Eur. Cer. Soc. 20, (2000), pp. 127/132.

[10] Zhang, J., and Desai, V., Evaluation of Thickness, Porosity and Pore Shape of Plasma Sprayed TBC by Electrochemical impedance spectroscopy, Surf. Coat. Tech. 190, (2005), pp. 98/109.

[11] Tomaszek, R., Nitsch, K., Pawlowski, L., Znamirowski, Z. and Brylak, M., Impedance Spectroscopy of Suspension Plasma Sprayed Titania Coatings, Surf. Coat. Tech. 201, (2006), pp. 1930/1934.

[12] Saenger, R., Martin, D., and Gabrielli, C., Electrochemical Characterization of Plasma Sprayed WC-CO Coatings by Impedance Techniques, Surf. Coat. Tech. 194, (2005), pp. 335/343.

[13] Morks, M.F., Cole, I., Corrigan, P., and Kobayashi, A., Electrochemical Characterization of Plasma Sprayed Alumina Coatings, J. Surf. Eng. Mat. Adv. Tech. 1, (2011), pp. 107/111.

[14] McCluney, S.A., Popova, S.N., Popov, B.N., and White, R.E., Comparing Electrochemical Impedance Spectroscopy Methods for Estimating the Degree of Delamination of Organic Coatings on Steel, J. Electrochem. Soc. 139, (1992), Issue 6, pp. 1556/1560.

[15] Loveday, D., Peterson, P., Rodgers, B., Evaluation of Organic Coatings with Electrochemical Impedance Spectroscopy, JCT CoatingsTech, (2004), pp. 88/93.

[16] Toma, F.-L., Scheitz, S., Berger, L.-M., Sauchuk, V., Kusnezoff, M., and Thiele, S., Comparative Study of the Electrical Properties and Characteristics of Thermally Sprayed Alumina and Spinel Coatings, J. Therm. Spray Technol. 20, (2011), Issue 1-2, pp. 195/204.

[17] Abelard, P., and Baumard, J.F., Electrical and Dielectric Properties of Forsterite Between 400 and 900°C, Phys. Earth Plan. Int. 23, (1980), pp. 98/102.